Changes in spectral shape of tissue optical properties in conjunction with laser-induced thermotherapy

Nilsson, A. M. K.; Sturesson, Christian; Liu, D. L.; Andersson-Engels, Stefan

Published in:
Applied Optics

1998

Changes in spectral shape of tissue optical properties in conjunction with laser-induced thermotherapy

Annika M. K. Nilsson, Christian Sturesson, David L. Liu, and Stefan Andersson-Engels

We measured the optical properties on samples of rat liver tissue before and after laser-induced thermotherapy performed *in vivo* with Nd:YAG laser irradiation. This made it possible to monitor not only the influence of coagulation on the scattering properties but also the influence of damages to vessels and heat-induced damage to blood on the absorption properties. An experimental integrating-sphere arrangement was modified to allow the determination of the g factor and the absorption and scattering coefficients versus the wavelength in the 600–1050-nm spectral region, with the use of a spectrometer and a CCD camera. The results show a relative decrease in the g factor of on average 21 ± 7% over the entire spectral range following thermotherapy, and a corresponding relative increase in the scattering and absorption coefficients of 23 ± 8% and 200 ± 100%, respectively. An increase of on average 200 ± 80% was consequently found for the reduced scattering coefficient. The cause of these changes in terms of the Mie-equivalent average radius of tissue scatterers as well as of the distribution and biochemistry of tissue absorbers was analyzed, utilizing the information yielded by the g factor and the spectral shapes of the reduced scattering and absorption coefficients. These results were correlated with the alterations in the ultrastructure found in the histological evaluation. The average radius of tissue scattering centers, determined by using either the g factors calculated on the basis of Mie theory or the spectral shape of reduced scattering coefficients calculated on the Mie theory, was estimated to be 21–32% lower in treated than in untreated liver samples. The Mie-equivalent average radii of scattering centers in untreated liver tissue deduced by the two methods corresponded well and were found to be 0.31 and 0.29 μm, respectively, yielding particle sizes in the same range as the size of a mitochondrion.

OCIS codes: 140.3460, 170.1420, 170.3890, 170.6930.

1. Introduction

Knowledge concerning the distribution of light in tissue is essential in conjunction with all clinical thermal treatments employing laser light, among others hyperthermia, obliteration of port-wine stains, laser surgery, etc., to control and optimize the resulting heat deposition and thus the result of the treatment. The transport of light in tissue is governed by irradiation and tissue geometry as well as by the optical parameters of tissue such as its refractive index n, its scattering asymmetry (or anisotropy) factor g, its scattering coefficient μ_s, and its absorption coefficient μ_a. The optical scattering parameters, i.e., the g-factor and the scattering coefficient, are defined as the average cosine of the photon scattering angle and the probability of photon scattering per unit path length, respectively. The effective scattering is often quantified by weighting the scattering coefficient with an angular scattering factor to yield the reduced scattering coefficient, $\mu_s' = \mu_s(1 - g)$. The optical absorption parameter, i.e., the absorption coefficient, is defined as the photon absorption per unit path length.

All the properties mentioned, together with the thermal properties of tissue, constitute input parameters for simulation programs based on a variety of theoretical models for light and heat distribution[1–5] used to analyze light and heat dosimetry in conjunction with laser-induced thermotherapy. However, these static models assume constant optical properties, whereas laser-induced heating causes severe morphological damage to the tissue, such as denaturation of structural proteins and tissue and cellular edema.[6] Morphological changes in the tissue matrix affect the optical properties and thus the light distribution, as was theoretically shown by Rastegar and

The authors are with the Department of Physics, Lund Institute of Technology, P.O. Box 118, S-221 00 Lund, Sweden.

Received 12 May 1997; revised manuscript received 6 October 1997.

0003-6935/98/071256-12$15.00/0

Motamedi.[7] They employed a dynamic light–heat distribution model based on the solution of the heat conduction equation with a temperature-dependent term for the laser heat source, which was deduced using the one-dimensional light diffusion approximation with linear temperature-dependent absorption and scattering properties. Significant differences in the resulting heat deposition were obtained, compared with those found on the assumption of constant optical properties. In practice, an increase in the reduced scattering coefficient versus temperature has been measured *in vitro* in all previously performed studies on tissue that had undergone slow heating by sources other than lasers, while the behavior of the absorption coefficient was less consistent.[8–14] The absorption coefficient is influenced mainly by light absorption by blood as hemoglobin is one of the main absorbers in tissue in the visible wavelength range. Thus the inconsistency in the results is probably a result of different blood content that is due to different experimental procedures. As μ_a plays a major role in the heat source term for the thermal distribution, a change in this parameter is of particular importance in connection with laser-induced thermotherapy and must be analyzed in a consistent way.

The primary aim of this study was to gain a more complete picture of the changes in the optical properties in conjunction with thermotherapy and their effect on the distribution of the light used for the treatment. Thus, we investigated the influence of tissue matrix coagulation on the scattering parameters as well as to what extent heat-induced damage to the blood[15] and the microvasculature[16] affects the average absorption coefficient in conjunction with laser-induced thermotherapy on organs *in vivo*. This was necessary as damage to the microvasculature was previously shown to have a major effect on the average absorption coefficient of tissue, albeit in conjunction with photodynamic therapy.[17]

A widely used technique to determine the three optical properties, g, μ_s, and μ_a, is that based on measurements using an integrating sphere[18] that involves recordings of the diffuse reflectance, the diffuse or total transmittance, and the collimated transmittance. The three parameters can be measured either consecutively with a single integrating sphere as in this study or simultaneously with a double integrating sphere.[19,20] The latter experimental arrangement provides an elegant technique for monitoring time-dependent changes in optical properties caused by any external stimulus. However, since no time-dependent phenomena were studied here, there was no advantage in using a double integrating sphere.

Employing the integrating-sphere approach, the optical properties are often either determined at one single wavelength with a monochromatic light source or at a few individual wavelengths by use of white light in combination with a monochromator as the light source. However, more complete information on the spectra is clearly desirable when studying possible biochemical changes in characteristic biological molecules such as hemoglobin, as well as to gain information about changes in the average size of scattering centers in the tissue matrix due, for example, to coagulation. The latter was in this study evaluated by forming a Mie-equivalent average radius and utilizing two different methods for comparison. One of the two estimations of the scattering size, which employs the spectral shape of reduced scattering coefficients calculated on the Mie theory, has previously been reported by Mourant *et al*. and has been successfully applied to tissue phantoms.[21]

Our second aim was to study the above mentioned microscopic properties of tissue by means of their spectral effect on the optical properties measured macroscopically in conjunction with laser-induced thermotherapy. To correlate the results with those reported in the histological analysis, we have developed an integrating-sphere arrangement that makes possible measurements of the spectral behavior of the optical properties over a wide spectral range, achieved simply with only three measurements.

2. Material and Methods

A. Sample Preparation and Irradiation

In all, 21 liver samples were harvested from 12 inbred Wistar–Furth female rats. The animals were allowed free access to an ordinary diet of pellets and tap water before the experiments, carried out in accordance with protocols approved by the local ethics committee for experimental animals. The animals were anesthetized with 5% chloral hydrate (250 mg/kg body weight) intraperitoneally. The abdomen was opened and the left liver lobe was exposed and put onto a few layers of gauze soaked in normal saline. A continuous wave Nd:YAG laser (Model 416, Quantronix Corporation, Smithtown, New York), emitting radiation at 1064 nm, was utilized to induce thermotherapy. The laser light was guided by a 600-μm quartz fiber and the polished end face of the fiber was imaged with a microscope objective lens giving 40$\times$ magnification onto a spot 1 cm in diameter on the surface of the liver. This yielded an irradiation intensity of 2.5 W/cm^2, resulting in a top-hat uniform-light-intensity distribution. The spot size was measured by employing an infrared sensing card. Tissue surface dehydration was avoided by maintaining the liver surface slightly moistened during the illumination with a small amount of saline at room temperature. The temperature approximately 3 mm below the surface of the liver was measured at the center of the irradiated spot with a thermistor 0.6 mm in diameter (Model 511, Yellow Springs Inc., Yellow Springs, Ohio) connected to an analog-to-digital converter and a personal computer. Temperature recordings were made every other second during the treatment. Laser-induced thermotherapy was applied for 20 min, raising the temperature of the tissue to 57.7 $\pm$ 5.9 °C (mean $\pm$ one standard deviation). The illuminated area of the tissue darkened after a few minutes, with a surrounding paler

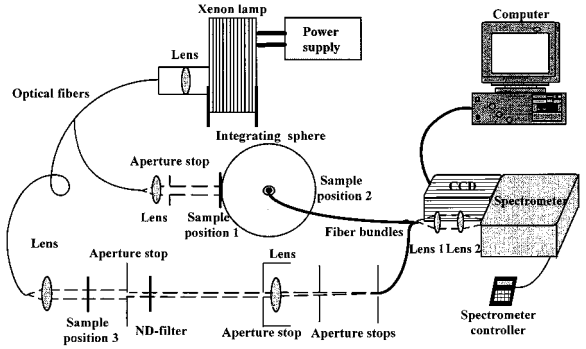

Fig. 1. Experimental setup consisting of two arrangements used to determine the optical properties of tissue. The integrating sphere and the narrow beam arrangements share the same light source, a Xe lamp, and the detector, a CCD camera mounted on a spectrometer. Total transmittance and diffuse reflectance spectra could be measured when tissue samples were placed in positions 1 and 2. Collimated transmittance spectra could be acquired when the samples were positioned in position 3.

peripheral region with a radius of approximately 4 mm. Outside this area with a total diameter of approximately 1.8 cm the liver tissue remained unchanged to the naked eye.

Directly after the treatment the illuminated left liver lobe was excised and the optical properties were measured. Immediately following these measurements, the right untreated liver lobe was excised and examined in the same way. The animals were then sacrificed by an overdose of the anesthetic drug. For the measurements all samples were prepared by cutting a thin superficial slice ~1.5 mm thick, parallel to the surface of the liver, and including the irradiated spot in the case of the treated samples. The slice was placed between two glass slides 1.0 mm thick, separated by two 1.0-mm spacers. By applying gentle pressure to the glass slides the liver sample was easily compressed to a thickness of 1.0 mm. The size of the sample between the glass slides was approximately 3 × 3 cm. This routine was repeated for 10 of the 12 animals, resulting in 9 treated samples and 10 untreated samples, as one treated sample had to be excluded because of suspected dehydration of the tissue surface. The remaining two rats were illuminated as described above, resulting in two additional treated liver samples. These two samples were fixed in 4% formaldehyde and analyzed histologically by a pathologist.

B. Measurements of Optical Properties

Measurements of the total and collimated transmittance as well as diffuse reflectance were accomplished with an integrating-sphere technique utilizing the system shown in Fig. 1. The setup consists of two optical arrangements. One consists of the integrating sphere (Oriel Corporation, Stratford, Connecticut), which is a sphere with an inner surface covered by highly diffusely reflecting barium sulphate that collects the transmitted light flux from a thin tissue sample placed in sample position 1 and the diffusely reflected light flux when the sample is placed in sample position 2. With the area of the sample port small relative to the total area of the sphere (here ~0.3%), we can assume that the light losses are approximately the same for a tissue sample as for the calibration standard used in the reference measurement. The integrating-sphere theory[18] can then be reduced to the following expressions for the reflectance and transmittance

$$R(\lambda) = R_{\mathrm{BS}}(\lambda) \times [I_R(\lambda)/I_{\mathrm{ref}}(\lambda)], \quad (1)$$

$$T(\lambda) = I_T(\lambda)/I_{\mathrm{ref}}(\lambda), \quad (2)$$

where $I_R(\lambda)$ is the measured intensity at a specific light wavelength λ with the sample at sample position 2, and $I_T(\lambda)$ is the corresponding measured intensity with the sample at position 1 and a barium sulphate plug at position 2. The reference intensity $I_{\mathrm{ref}}(\lambda)$ is measured when the reflected light flux, resulting from a barium sulphate plug at sample position 2, fills the sphere without interacting with any samples. The barium sulphate plug was a calibration standard with a wavelength-dependent reflectance factor $R_{\mathrm{BS}}(\lambda)$ certified by the National Institute of Standards and Technology. A calibration series consisting of calibration standards with reflectance factors of approximately 2%, 50%, 75%, and 99% confirmed the hypothesis that Eqs. (1) and (2) were applicable, yielding measurement errors of ±2% for the 2% calibration standard and ±1% for the 50%, 75%, and 99% standards.

The second optical arrangement, shown in the lower part of Fig. 1, was used to measure the collimated transmittance of the sample placed at sample position 3. The collimated transmittance refers to the light passing straight through the sample without interaction between light and tissue, according to the Beer–Lambert law. The intensity of this nonscattered and nonabsorbed light, $I_{\mathrm{col}}(\lambda)$, can thus be expressed as

$$I_{\mathrm{col}}(\lambda) = I_0(\lambda)/T_{ND}(\lambda)\exp\{-[\mu_a(\lambda) + \mu_s(\lambda)]d\}, \quad (3)$$

where $I_0(\lambda)$ is the intensity of the reference light, measured in the same geometry, with the tissue sample replaced by a thin water-filled reference glass cell and attenuated by neutral density filters with the total transmittance factor $T_{\mathrm{ND}}(\lambda)$. The thickness of the water sample was 1 mm, the same as the tissue sample. The neutral density filters (Schott, Mainz, Germany) were used for the reference measurements $[I_0(\lambda)]$ to limit the required dynamic width for the detection by acquiring water cell intensities as well as tissue sample intensities in the same range, thus minimizing nonlinear effects in the detection. Measuring the collimated transmittance allowed us to determine the sum of the absorption and scattering coefficients, i.e., the total interaction coefficient $\mu_t = \mu_a + \mu_s$ by applying Eq. (3).

Both optical arrangements have the same light source and detector. A 75-W high-pressure xenon lamp generating white light (Osram, Berlin, Germa-

ny) was used as a light source, and the light was focused into two optical fibers with core diameters of 600 μm. The first fiber guided the light to the integrating sphere. A light beam with a diameter of approximately 4 mm was formed at both sample positions of the sphere by means of a lens and an aperture stop at the distal end of the fiber. The second fiber guided the light to the collimated transmittance setup, where a lens and several aperture stops formed a collimated beam with a diameter of approximately 5 mm that passed straight through the sample as shown in Fig. 1. The tissue sample was placed just in front of an aperture located 35 cm from a second aperture (8 mm in diameter as the beam was slightly divergent) that filtered out scattered light. Finally, a light-probing fiber bundle placed 50 cm from the second aperture guided the collected light to a spectrometer (270M, SPEX Industries Inc., Edison, New Jersey). The probing light from the integrating sphere was collected by a second fiber bundle similar to that in the narrow beam setup. The diameter of the fiber bundles was approximately 5 mm. The probing light from each fiber bundle was separately imaged onto the entrance slit of the spectrometer by two lenses and spectrally resolved by a 150-g/mm grating blazed at 500 nm. A cooled CCD camera (CCD 1100PB, EG&G Princeton Instruments Inc., Princeton, New Jersey) with 1100 × 330 pixels was mounted at the exit plane of the spectrometer. With this setup all wavelengths between 600 and 1050 nm could be detected at a spectral resolution of 4 nm. Wavelength calibration of the detector was performed with mercury and xenon calibration lamps with a precision estimated to be ±1 pixel (0.5 nm). Background spectra were acquired before each measurement and automatically subtracted.

The calibration of the integrating-sphere arrangement, when the calibration standards mentioned above, were used, was combined with calibration measurements on a suspension of latex spheres 2 μm in diameter, yielding scattering properties similar to those obtained for liver tissue. The g factors and scattering properties measured were compared with Mie-calculated values, as performed in Ref. 17, and resulted in good agreement to within ±6% in the entire wavelength range studied (600–1050 nm).

We measured three parameters, i.e., the sum of the absorption and scattering coefficients, the total transmittance, and the diffuse reflectance, and were able to deduce the three optical properties, g, μ_s, and μ_a, by fitting the measured parameters to results of Monte Carlo simulations.[22] In this case, in which three parameters for each tissue sample were to be deduced for many wavelengths, a fast algorithm was necessary. Therefore, a data base of results of Monte Carlo simulations was built up before the measurements. The optical properties were then evaluated from the measured values by spline interpolations.[17] This new experimental approach with multiwavelength detection enabled us to determine a complete set of optical properties, g, μ_s, and μ_a, versus the wavelength in only three measurements, compared with the many measurements needed when probing one wavelength at a time with a monochromator setup.[10,17,20,23]

Three measurements performed on each liver sample were completed within 25 min after resection and resulted in a total of 57 spectra (600–1050 nm) of each optical parameter of the tissue g, μ_s, and μ_a. Thirty measurements were performed on 10 untreated liver samples, 15 measurements were made on the darkened treated central area, and 12 on the paler peripheral region of the remaining nine treated samples included in the study.

C. Simulations of Light Dose Distribution in Liver Tissue

The effect of heat-induced changes in the optical properties on the light dose delivered was analyzed by simulating the light flux distribution of the treatment light in a liver sample before and after completed thermotherapy, applying Monte Carlo computations.[22] Assuming no major differences in the optical properties at 1050 and 1064 nm, the average optical properties obtained at 1050 nm were used as input data. The irradiation geometry utilized was a beam with a top-hat distribution, a 0.5-cm radius as in the experiments, and a postulated total energy of 1 J.

D. Spectral Analysis of Optical Properties

When comparing the spectral shapes of the optical properties measured on treated and untreated tissue, we gain information about possible biochemical and morphological changes induced by the treatment. To visualize the spectral changes in the absorption coefficient that were due to the treatment, the absorption spectrum obtained from the untreated liver lobe was subtracted from that measured on the treated liver lobe of the same rat, forming $\Delta\mu_a$ spectra.

Morphological changes in the tissue were analyzed employing computations based on Mie theory, forming a Mie-equivalent average radius of the tissue scattering centers in treated and untreated liver tissue. The analysis was based either on the deduced g factor or on the spectral shape of the reduced scattering coefficient. The strong dependence of the g factor on particle size is well known, and the purpose of the first analytical approach was to quantify this relationship by employing computations based on Mie theory for different particle sizes.[24] We performed 230 Mie computations for spherical particles with a radius between 0.015 and 0.6 μm in the 600–1050-nm wavelength range, all with a refractive-index ratio of 1.037 (the refractive index of the particle divided by that of the surrounding medium equals 1.4/1.35) typical of biological cells.[21] The g factors were averaged over the wavelength and plotted versus particle radius. To obtain an expression for the dependence of the g factor as a function of particle size, two third-order polynomials were fitted to the calculated g factors. By inserting the average g factors measured for treated and untreated liver tissue in this fitted polynomial expression, an esti-

mation of the mean size of the scattering centers in the tissue, the Mie-equivalent radius could be obtained.

Furthermore, the spectral shape of the reduced scattering coefficient was also utilized to estimate the Mie-equivalent average radius of tissue scatterers by assuming the following wavelength dependence:

$$\mu_s'(\lambda) = k\lambda^n, \tag{4a}$$

or rearranged as

$$\ln[\mu_s'(\lambda)] = \ln(k) + n\ln(\lambda), \tag{4b}$$

suggested by Mourant *et al.*[21] as a consequence of a similar dependence for the reduced efficiency factor Q_s' of a single scatterer

$$Q_s' \sim \lambda^n, \tag{5}$$

assuming independent scattering in the sample with the associated, macroscopic, reduced scattering coefficient μ_s'. Independent scattering implies that the macroscopic scattering is simply deduced by multiplying the individual scattering efficiency factor with the number density N and the cross-sectional area A of the scattering particles in the sample:

$$\mu_s' = NAQ_s', \tag{6}$$

from which Eq. (4) follows. The validity of Eq. (5) has been investigated by Graaf *et al.*[25] for scattering particles with refractive-index ratios m, typical of biological cells ($1 < m < 1.1$). They revealed that the wavelength exponent n in Eq. (5) approaches -0.37 for larger particle radii r relative to the wavelength of the scattered light in the medium λ_m. In other words, for particles with larger size parameters, $x = 2\pi r/\lambda_m$, in the range 5–50. For smaller size parameters ($x < 1$) n approaches -4, the well-known Rayleigh proportionality.[26] Employing Mie theory calculations, Mourant *et al.*[21] report wavelength exponents n between -4 and -0.37 for particles with intermediate radius, suggesting that n depends on the particle size. From this it follows that the spectral shape of the reduced scattering coefficient, i.e., the slope of μ_s' versus the wavelength as a ln–ln plot [see Eq. (4b)], depends on the particle size. The average size of scattering centers in tissue can thus be estimated by extracting this slope coefficient from measured μ_s' spectra if the size dependence of the wavelength exponent, $n = n(r)$, is known.

A simple approximation of $n = n(r)$ was formed by calculating Q_s' versus the wavelength between 600 and 1050 nm for 23 different scattering particles with a radius in the 0.015–0.6-μm range, employing the results of the Mie theory computations previously mentioned. By plotting the natural logarithm of the Q_s' values computed on the Mie theory versus the natural logarithm of the corresponding wavelength and introducing a linear regression fit, a slope coefficient corresponding to the wavelength exponent n was deduced for each particle size. Twenty-three different slope coefficient–particle radius pairs were thus obtained, and two third-order polynomial fits were used to express the size dependence of the wavelength exponent $n = n(r)$. According to Eqs. (5) and (6), a slope coefficient obtained from a measured μ_s' spectrum corresponds to a particle radius via the derived polynomial fits of $n = n(r)$. This radius was, as mentioned above, called the Mie-equivalent average radius. The Mie-equivalent average radius of scatterers in untreated liver tissue as well as in peripheral and central treated liver tissue was thus also estimated by extracting the ln–ln slope coefficients of the measured average μ_s' spectra obtained from each tissue group.

3. Results

A. Histological Evaluation

The histological analysis revealed a treatment volume consisting of three pathologically different layers with a total treatment depth of 4–5 mm. A macroscopically darkish central region was 9–10 mm in diameter and approximately 0.07 mm in depth. The darkish color originated from a considerable concentration of erythrocytes in the substantially enlarged liver sinusoids, which pressed the liver cells. The liver cells exhibited vacuole formation in the cytoplasm and damaged nuclei. The second layer was 0.2 mm thick with thinner sinusoids, but still composed of liver cells with damaged nuclei. The third layer exhibited again enlarged sinusoids but with fewer erythrocytes.

B. Optical Measurements

The collimated and total transmittance obtained, as well as the diffuse reflectance spectra, were averaged within each group, i.e., 30 sets of spectra from untreated liver samples, 15 sets of spectra from the darkened treated central area, and 12 from the paler peripheral region. The resulting average spectra are shown in Fig. 2 with error bars indicating the standard deviations. The collimated and total transmittance spectra [Figs. 2(a) and (b)] obtained from treated areas clearly display lower signals in the entire wavelength range than those obtained from untreated samples. Treated central regions exhibit even lower signals than peripheral regions. The differences in the reflectance spectra, shown in Fig. 2(c), are less apparent. Average spectra from untreated samples tend to exhibit lower diffuse reflectance than treated areas, though there is an overlap when the standard deviations are included. The central and peripheral treated regions do not differ significantly. No characteristic spectral features can be observed in this wavelength range (600–1050 nm) apart from the influence of the tail of the absorption peak of oxyhemoglobin at 577 nm. All recordings thus demonstrate lower signals at shorter wavelengths. The small ripples in the spectra are artifacts within the standard deviations, partly originating from a slightly nonlinear sensitivity of the detector observed as a result of manifest characteristic peaks in the xenon lamp spectrum.

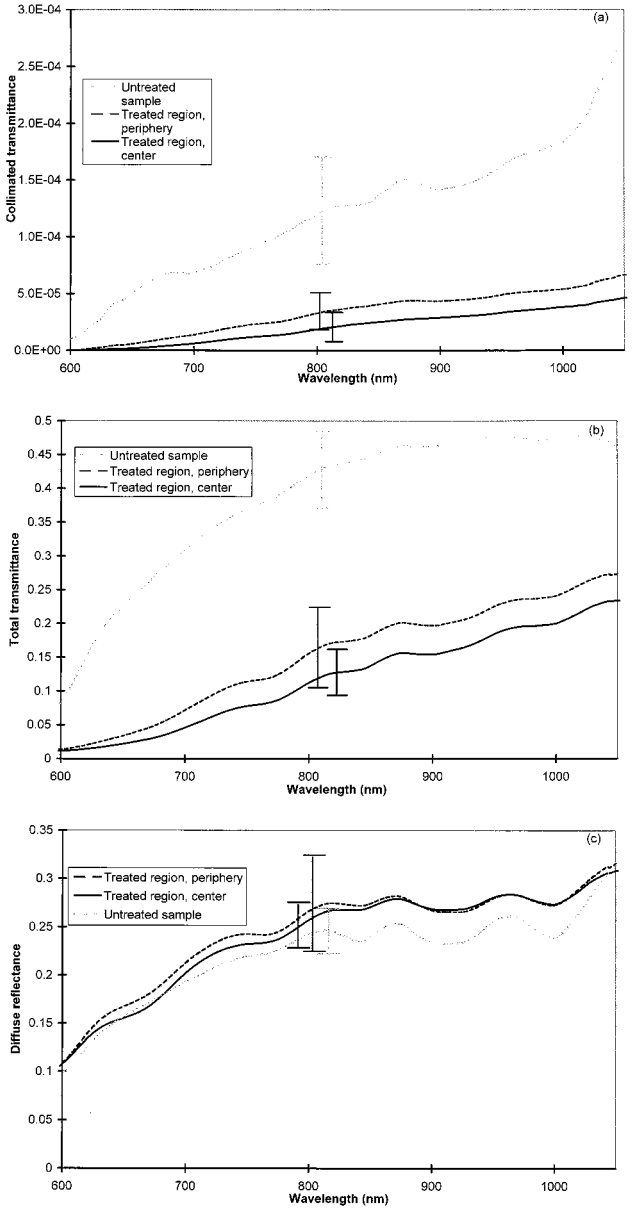

Fig. 2. Average spectra of (a) collimated transmittance, (b) total transmittance, and (c) diffuse reflectance, versus the wavelength in the range 600–1050 nm, based on 30 spectra obtained from untreated tissue, 12 spectra from treated peripheral regions, and 15 spectra from treated central regions. The error bars represent the standard deviations evaluated at 825 nm within each group. The standard deviations were found to be approximately the same in the entire spectral region shown.

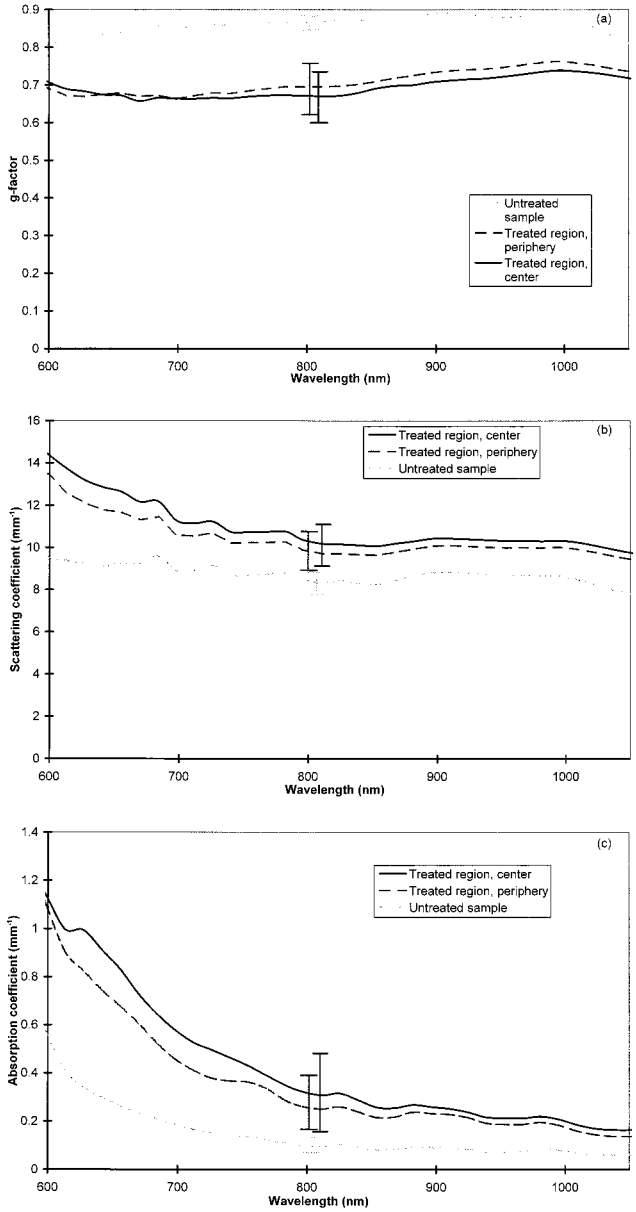

Fig. 3. Average spectra of the three optical properties versus the wavelength (600–1050 nm): (a) the g factor, (b) the scattering coefficient, (c) the absorption coefficient. The error bars represent the standard deviations evaluated at 825 nm, which were approximately the same over the entire spectral region shown.

The corresponding average spectra of the three optical properties are shown in Fig. 3. They are based on 57 sets of $g/\mu_s/\mu_a$ spectra obtained from an equal number of runs of the spline interpolation program, which performs interpolations in the Monte Carlo data base. Figure 3 demonstrates that the g factor is fairly independent of the wavelength, whereas both the scattering and absorption coefficients depend significantly on the wavelength, the former being influenced by the average size of the scattering centers in the tissue and the latter mainly by the light absorption in blood. An additional general observation from Fig. 3 is that the optical properties obtained from the treated samples differ significantly in the entire wavelength range from those obtained from untreated samples, while only insignificant differences between treated central and peripheral regions can be observed. The g factors of treated liver samples are clearly lower than those of untreated samples [Fig. 3(a)]. In an individual comparison of the three g spectra from an untreated sample with those from a treated sample obtained from the same animal, the central treated regions exhibit an average

decrease in the g factor of 21 ± 7% (±1 standard deviation) and 19 ± 8% in the peripheral regions.

The scattering coefficients of the treated samples, shown in Fig. 3(b), are significantly higher than those of the untreated samples over the entire spectral range. There is also a tendency, though insignificant, of higher μ_s coefficients for the central treated region compared with those obtained for the peripheral region. The scattering coefficients were on average 23 ± 8% and 18 ± 9% larger in the treated central and peripheral regions, respectively, in comparison with those in the untreated samples. The change in the effective scattering was also analyzed by evaluating the reduced scattering coefficients for all 57 spectra. The reduced scattering coefficients in the treated central and peripheral regions were on average 200 ± 80% and 180 ± 100% higher than in untreated samples, respectively. Finally, the average spectra of the absorption coefficients including the standard deviations, shown in Fig. 3(c), reveal increasing absolute values with shorter wavelengths that are due to the light absorption by blood, irrespective of sample group. The treated samples clearly exhibit higher absorption coefficients than the untreated samples, with the treated central region slightly higher than the peripheral region. Subtracting untreated from treated absorption spectra results in $\Delta\mu_a$ spectra, all with a shape similar to that of the spectra of the absolute values. Hence, the relative differences in the absorption coefficient were more or less independent of wavelength; 200 ± 100% and 180 ± 80% higher in the treated central and peripheral regions than in the untreated samples, respectively.

C. Monte Carlo Simulations

The light flux distributions of the treatment light in a liver sample before and after completed treatment were simulated by using as input data the average optical properties obtained at 1050 nm for the untreated samples $g = 0.81$, $\mu_s = 7.7\ \text{mm}^{-1}$, and $\mu_a = 0.06\ \text{mm}^{-1}$, as well as for the treated central sample areas $g = 0.72$, $\mu_s = 9.7\ \text{mm}^{-1}$, and $\mu_a = 0.16\ \text{mm}^{-1}$. The two resulting light dose distributions delivered are shown as contour plots versus radius (0–1.5 cm) and tissue depth (0–1.0 cm) in Fig. 4, with the untreated liver sample displayed on the right-hand side and the treated sample on the left-hand side of the diagram. The penetration depth of the treatment light is apparently significantly reduced after treatment. The penetration depth expressed in diffusion theory terms, $\delta = \{3\mu_a[\mu_a + \mu_s(1 - g)]\}^{-1/2}$, is reduced from 1.9 to 0.85 mm, i.e., to approximately 45% of the value of untreated tissue.

D. Spectral Analysis of Optical Scattering Properties

A measure of the induced morphological changes in tissue by thermotherapy was deduced by estimating the Mie-equivalent average radius, previously defined. The Mie-equivalent average radius was evaluated from the g factors as well as from the spectral behavior of the reduced scattering coefficient. The

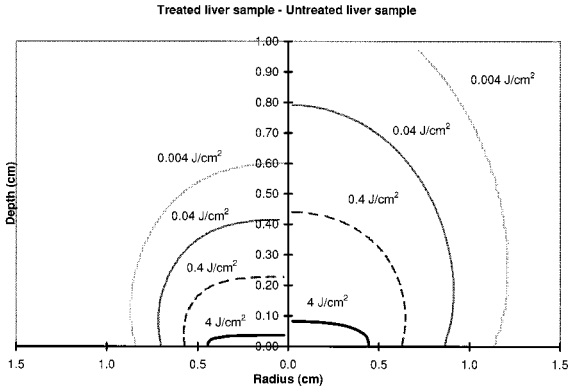

Fig. 4. Monte Carlo-simulated light fluence of the treatment light (1064 nm) with the average optical properties measured for liver samples before and after completed treatment as input parameters. The results are shown as contour plots versus radius and tissue depth, with the untreated liver sample on the right-hand side and the treated sample on the left.

theoretical particle size dependence of the g factor is shown in Fig. 5 as g factors computed on the Mie theory, averaged over the 600–1050-nm wavelength range, versus particle radius. Two polynomial functions, also shown in Fig. 5, were fitted to the data in two regions. The functions describe the theoretical relationship between the g-factor and the particle radius as

$$g = -105.41r^3 + 43.798r^2 - 1.2922r + 0.0108 \quad (r \leq 0.20\ \mu\text{m}), \quad (7)$$

$$g = 4.7171r^3 - 7.5211r^2 + 4.2136r + 0.0996 \quad (0.20 < r \leq 0.60\ \mu\text{m}). \quad (8)$$

The measured g factors, averaged over all samples and over the wavelength range studied (600–1050 nm), were $g = 0.82 \pm 0.04$ for untreated liver tissue,

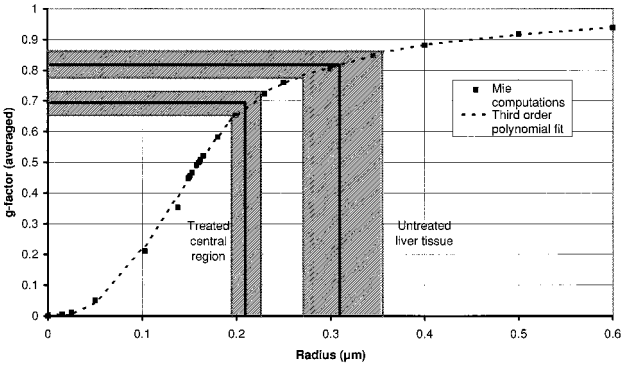

Fig. 5. Mie-theory-computed g factors averaged over the wavelength range used (600–1050 nm) versus particle radius represented by rhombic symbols. The dashed curve is the approximation composed of two third-order polynomial fits used to estimate the Mie-equivalent average radius from the measured average g factors. The black lines represent measured mean g factors ± 1 standard deviation and their corresponding Mie-equivalent average radii.

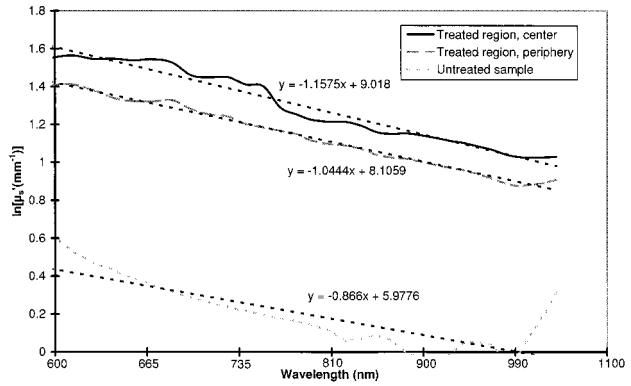

Fig. 6. Average spectra of the reduced scattering coefficient as a ln–ln plot. The solid black and the grey dashed curves represent average spectra for treated central and peripheral tissue, respectively, and the grey dotted curve the untreated tissue. A linear regression fit was formed to each average spectrum, shown as an adjacent black dashed curve, exhibiting lower slope coefficients for treated tissue (−1.16 and −1.04) than for untreated tissue (−0.87). This indicates a smaller average size of scattering centers in treated tissue.

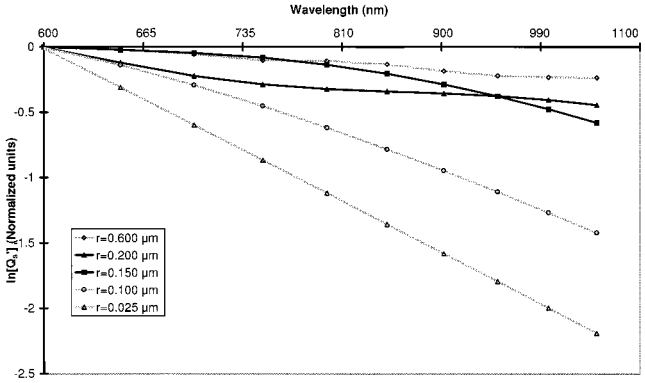

Fig. 7. Examples of Mie-computed Q_s' spectra as ln–ln plots for five particle sizes, revealing lower slope coefficients for smaller particles. All lines were normalized to 0 at 600 nm to illustrate clearly the difference in slope coefficients. Spectra obtained from particles with intermediate size (r = 0.150 and 0.200 μm) are represented by solid black lines to expose the slight divergence from the assumed linear ln(λ) dependence.

$g = 0.71 \pm 0.03$ for treated peripheral tissue, and $g = 0.70 \pm 0.03$ for treated central tissue. The estimated Mie-equivalent average radii were thus 0.31 μm (0.27–0.36 μm including the standard deviations of the g-factor) for untreated liver tissue, 0.22 μm (0.20–0.24 μm) for treated peripheral tissue, and finally 0.21 μm (0.19–0.23 μm) for treated central tissue, i.e., a decrease in the Mie-equivalent size of 29 and 32% in the treated compared with in the untreated tissue.

The spectral shape of the reduced scattering coefficient was also used to estimate the Mie-equivalent average radius by employing a polynomial approximation of the ln(Q_s')-slope coefficient, $n = n(r)$. Figure 6 shows the measured average μ_s' spectra for the three tissue groups in a ln–ln plot and corresponding linear regression fits yielding the μ_s'-slope coefficients. The wavelength exponent n was thus estimated to be −0.87 for untreated liver tissue, −1.04 for treated peripheral tissue, and −1.16 for treated central tissue.

Mie computations of Q_s' spectra were performed in the wavelength range studied (600–1050 nm) for 23 particles with a radius between 0.015 and 0.60 μm. Five examples of ln(Q_s') plotted versus ln(λ) are shown in Fig. 7. For the comparison of the slopes, all curves were normalized to 0 at 600 nm. A gradual decrease in the slope coefficient is shown for smaller particles, approaching the Rayleigh proportionality $n = -4$. Despite the fact that particles of intermediate size, represented by solid black lines in Fig. 7 (r = 0.15 and 0.20 μm), appear to deviate from a straight line [revealing that Eq. (5) is not completely true in this particle range], a linear regression fit was introduced in all 23 Mie-computed Q_s'-spectra. However, for the intermediate-sized particles (r = 0.15–0.20) this fit was based on a subset of deduced values at wavelengths higher than 750 nm (the first three Mie-computed values were excluded in each series) owing to this nonlinearity. This wavelength subrange appeared to yield reasonable slope coefficients for the intermediate-sized particles, fitting the general trend given by smaller and larger particles. All corresponding slope coefficients were deduced and are presented versus the particle radius in Fig. 8. A mathematical expression, $n = n(r)$, was derived by fitting two polynomials, one for the small and intermediate-sized particle region

$$n = -1109.5r^3 + 341.67r^2 - 9.3696r - 3.9359 \quad (r < 0.23\ \mu m), \quad (9)$$

and one for the larger particle region

$$n = 23.909r^3 - 37.218r^2 + 19.534r - 3.965 \quad (0.23 \le 4 < 0.60\ \mu m). \quad (10)$$

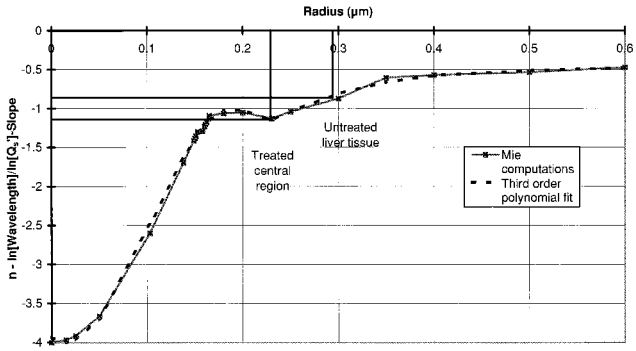

Fig. 8. Deduced slope coefficients from the Q_s'-spectra calculated on the Mie theory, as shown in Fig. 7, corresponding to the wavelength exponent n versus the particle radius. A mathematical fit was deduced, composed of two polynomials of the third order, and is represented by the dashed curve. The slight hump in the range r = 0.15–0.20 μm can be explained by an overestimation of the wavelength exponent, as the linear regression fit is not optimal for these intermediate-sized particles, as shown in Fig. 7.

The resulting fit is shown in Fig. 8 and corresponds well to the theoretical values obtained from Mie calculations.

The Mie-equivalent average radii corresponding to the slopes obtained from measured μ_s' spectra (-0.87, -1.04, and -1.16) were estimated by means of iteration of Eq. (10) to be 0.29 μm for the untreated liver tissue, 0.25 μm for the treated peripheral tissue, and 0.23 μm for treated central tissue, i.e., a 14% and 21% lower Mie equivalent average radius in the treated peripheral and central region, respectively, compared with untreated tissue.

4. Discussion

The possibility of acquiring a complete spectrum of the diffuse reflectance, and total and collimated transmittance, with a CCD detector connected to a spectrometer enables us to investigate conveniently whether there are any wavelength-dependent variations in the optical properties with higher accuracy and spectral resolution than by scanning the signal one wavelength at a time. This is essential, especially when the influence of biochemical and morphological properties on the optical properties is to be studied. Though absolute values do not play a central part in this study, it is reassuring to obtain calibration results with fairly small deviations as well as optical properties exhibiting similar spectral shapes and absolute values as those presented in previous studies.[17,23]

From the average spectra of the raw data shown in Fig. 2, we conclude that the total and collimated transmittance spectra exhibit more pronounced differences between treated and untreated samples than do the diffuse reflectance. This observation does not speak in favor of real-time monitoring of the treatment response in terms of changes in diffuse reflectance. However, a higher amount of diffusely backscattered light with a long scattering history is expected from bulk tissue than from a sample with a thickness of the order of the effective scattering length ($1/\mu_s'$). Thus the significant changes found in the total transmittance (including the diffuse part) of the treated samples can probably be observed in the backscattered light from tissue in clinical conditions. Yet experimental verifications are necessary to conclude this.

To deduce the optical properties we have employed results from Monte Carlo simulations that assume homogenous tissue samples. This assumed geometry is obviously not the best model for the treated liver sample, which exhibits three tissue layers with different histopathological ultrastructures according to the histological analysis, nor for the untreated liver sample composed of tissue matrix and capillaries containing blood. The optical properties obtained in this work are thus average values influenced by the optical properties of the tissue matrix as well as by optical properties and the distribution of hemoglobin and other chromophores. This is probably an explanation of the insignificant differences in the optical properties of tissue found in the treated central and peripheral regions, shown in Fig. 3, despite the distinct visual difference in color. These color alterations originate in the superficial central layer with enlarged sinusoids and erythrocytes in abundance observed in the histological analysis. The average optical properties were not significantly influenced by the optical properties in this layer owing to its small extension (0.07 mm) compared with the rest of the 1-mm-thick damaged tissue sample with less prominent color alterations.

However, significant differences in all three optical properties of treated versus untreated samples were found. The relative differences were independent of wavelength and were most pronounced for the absorption coefficient compared with the two scattering parameters. The twofold increase in the absorption coefficient reported here is significantly higher than the results obtained by others studying heating *in vitro*[9,10,12–14] with two exceptions, where the samples were carefully wrapped in water-tight aluminum foil before being heated in a water bath.[8,11] This inconsistency is thus probably a consequence of the experimental procedure. By performing the thermotherapy not on samples *in vitro* but on the tissue *in vivo*, we investigated the influence on the average optical properties of heat-induced coagulation of the tissue matrix as well as heat-induced damage to the microvasculature and blood, thus eliciting a more natural response to the treatment than might have been the case in earlier optical studies on heat-induced damage to tissue.[8–14] However, the actual measurements were performed on tissue *in vitro*, which implies a possible influence of, for example, the tissue deterioration postmortem on the absolute values of the optical properties. Yet, since the handling of both treated and untreated samples were the same, tissue degradation cannot explain the relative changes in the optical properties found in treated compared with untreated tissue. Furthermore, the twofold increase in the reduced scattering coefficient, mainly influenced by morphological damage in the tissue matrix, obtained in this study is in good accordance with the results in the previously mentioned studies. Our experimental approach did not permit the temperature dependence of the optical properties to be followed during the treatment. For this reason only irreversible changes in the optical properties were monitored. However, reversible changes may also arise during thermotherapy, such as those caused in connection with pulsed heating,[27] and they may influence the light distribution during the treatment. This phenomenon was not taken into account here.

It is interesting to compare the changes in the optical properties in conjunction with thermotherapy measured in this study with those obtained in conjunction with photodynamic therapy (PDT).[17] PDT normally also causes damage to the tissue microcirculation, changing the distribution of erythrocytes. This was earlier confirmed by a 30–40% average increase measured in the absorption coefficient.[17] However, in that study PDT hardly affected the scat-

tering properties, in contrast to the decrease in the g factor of on average 21% and the increase in the scattering coefficient of on average 23% as a result of thermotherapy shown in this work. This indicates a difference in treatment response and resulting morphological damage to the tissue matrix, probably related to the heat-induced denaturation in connection with thermotherapy, which does not occur in conjunction with the photochemical reactions caused by PDT.

The results of the Monte Carlo simulations, using the experimental optical properties of treated and untreated liver tissue at approximately the treatment wavelength of 1064 nm as input parameters, are shown in terms of light distribution versus sample radius and depth in Fig. 4. From this figure it is clear that the light penetration is less at the end of the treatment than at the beginning. This dynamic phenomenon of the optical properties should be accounted for in the theoretical and computational models for predicting the appropriate light and heat dosimetry in connection with thermotherapy.

The damage to the ultrastructure of the tissue caused by the thermotherapy was indirectly evaluated by analyzing the g factor, the spectral shapes of the reduced scattering coefficient, and the absorption coefficient. The hypothesis was that possible heat-induced biochemical changes in the biomolecules such as the hemoglobin would be reflected as characteristic changes in the spectra of the absorption coefficient, while changes in the distribution and concentration of absorbers would merely yield a constant relative change independent of wavelength. As there are no apparent spectral shifts in the absorption spectra, it is unlikely that the increasing absorption coefficient can be attributed to heat-induced biochemical damage. The wavelength-independent relative increase indicates instead that it is caused by changes in the distribution and volume concentration of hemoglobin, in good accordance with the observations made by the pathologist. The histological evaluation reports damage to the microvasculature. Such damage has also previously been observed by means of scanning electron microscopy.[16] The damage observed in the microvasculature, i.e., enlarged sinusoids with increased amount of erythrocytes, yields most likely a higher effective absorption coefficient. Furthermore, slowly heated blood has previously been shown to exhibit an exponential increase in its absorption coefficient with increasing temperature.[15] This was suggested to be caused by hemolysis, which may be an additional explanation.

Two methods were utilized to estimate heat-induced morphological changes in the tissue in terms of the Mie-equivalent average radius of the scattering centers in the tissue. Both methods were based on Mie theory computations. The first straightforward approach was an attempt to quantify the complex relationship between the size of scattering particles and the g factor, as shown in Fig. 5. The major approximation made here is that the Mie-computed g factors are averaged over the wavelength, since Mie theory predicts a wavelength-dependent g factor. However, this wavelength dependence is rarely measured for g factors of tissue and an averaging of the theoretical wavelength dependence thus seems appropriate. Once the relationship between the g factor and the particle radius is determined, a Mie-equivalent average radius corresponding to a measured g factor can be deduced by interpolation. The measured average g factors were rather high (untreated tissue, 0.82; treated peripheral tissue, 0.71; and treated central tissue, 0.70), implying large Mie-equivalent average sizes. Equation (8), valid for $0.20 < r \leq 0.60$ μm, was thus used to estimate iteratively the Mie-equivalent average radius, resulting in values in the range 0.21–0.31 μm. This method appears to be a simple and convenient approach to estimating the average size of scattering centers in tissue once the g factor of the tissue has been determined.

Since it is difficult to deduce the g factor, especially with measurement techniques applicable to tissue *in vivo*, we also wanted to try another method to estimate the Mie-equivalent average radius based on the slope of a more easily measured μ_s' spectrum as a ln–ln plot. This possibly more feasible approach, which was suggested and applied to tissue phantoms by Mourant *et al.*,[21] we further developed and applied to its full extent to liver tissue. Examples of results of Mie theory computations yielding Q_s' versus wavelength for particles in the 0.015–0.6-μm range, shown as ln–ln plots in Fig. 7, confirm the dependence of the slope on particle size as well as the deviation in $\ln(Q_s')$ from a linear $\ln(\lambda)$ dependence for intermediate particle size, previously shown in the work by Mourant *et al.*[21] This means that Eq. (5) must be regarded as only a rough approximation for particles in the 0.15–0.20-μm range. A mathematical fit composed of two polynomials was formed, one for the small and intermediate particle size region ($r < 0.23$ μm) and one for the larger particles ($0.23 \leq r \leq 0.60$). This implies that we must know approximately in which size range the average tissue scatterer lies to be able to utilize fully a μ_s'-spectrum to predict the Mie-equivalent average radius. Our measurements revealed a fairly high g factor, which suggests scattering by larger scattering centers. A good correspondence of the wavelength dependence of the measured μ_s' as a ln–ln plot (Fig. 6) to the linear regression fit was also obtained in contrast to the intermediate region, as previously discussed. We therefore employed Eq. (10) to estimate the Mie-equivalent average radius for treated and untreated tissue.

Both analytical methods, one straightforward based on the g factor, and one, possibly more feasible, based on the more easily measured parameter μ_s', yield similar results: 0.29 versus 0.31 μm for untreated tissue, 0.25 versus 0.22 μm for treated peripheral tissue, and finally 0.23 versus 0.21 μm for treated central tissue.

The estimated average radius of scattering centers in tissue must be considered as a scattering size index rather than a true absolute value of the physical size,

as we have assumed a wavelength-independent refractive-index ratio, m, and applied Mie theory as well as Eq. (6) to reach the simple expressions in Eqs. (7)–(10). The true wavelength dependence of m should not influence the results greatly according to Mourant *et al.*,[21] while the two latter approximations are of more serious concern. Mie theory assumes spherical scattering particles, a rough approximation for scattering in tissue, and Eq. (6) requires independent light scattering from individual particles, i.e., large interparticle spacings, which is far from being true in compact tissue. We thus prefer to call the estimated particle radius the Mie-equivalent average radius. However, Mourant *et al.*[21] have successfully used the $\log(\mu_s')$-slope to determine the average scattering particle size in Intralipid, often used as a tissue phantom, by applying Mie theory calculations. It is thus notable that the Mie-equivalent average radius for untreated liver tissue, employing both analytical approaches (0.29–0.31 μm), is in the same region as the size of a mitochondrion in liver tissue with an approximate radius in the range 0.25–0.5 μm. Beauvoit *et al.*[28] have also shown that the mitochondrial content in liver tissue is the predominant factor for light scattering.

It is interesting to observe that average μ_s'-spectra from treated tissue exhibit lower wavelength exponents ($n = -1.04$ and -1.16) than from untreated tissue ($n = -0.87$), indicating a lower average scatterer size in treated than in untreated tissue. This reduction in scatterer size index in conjunction with thermotherapy was supported by the histological analysis, which revealed heat-induced ultrastructural alterations in terms of the appearance of new aggregates that are due to coagulation and heat-induced vacuoles in the cytoplasm. It has previously been postulated that the number of scattering centers is increased, increasing the scattering coefficient, and the average particle size is decreased, yielding more isotropic light scattering and thus a reduced g factor,[8,10,29] which is supported both by our measurements and by our estimations.

5. Conclusion

In conclusion, we have shown that both scattering and absorption properties are affected by laser-induced thermotherapy. These changes reduce the penetration depth of the treatment light and influence the spatial distribution of the light dose delivered. Based on the wavelength-independent relative increase in the absorption coefficient in treated tissue and on the histological observations, we suggest that the twofold increase in the absorption coefficient can be related to the accumulation of erythrocytes that is due to heat-induced microvascular damage. Furthermore, the decrease in the g factor and the increase in scattering coefficient found in treated tissue are probably due to a decrease in the average size of the scattering centers as a result of heat-induced coagulation and vacuole formation in the cytoplasm. This was also confirmed by a decrease of approximately 21–32% in the Mie-equivalent average radius for treated tissue. The absolute value of this parameter was estimated to be 0.29–0.31 μm for untreated tissue, in accordance with the size of the suggested main scatterer in liver tissue, the mitochondrion. The Mie-equivalent average radius was thus shown to be an interesting parameter for the evaluation of tissue optics.

The authors thank Emma Johansson for valuable assistance and U. Stenram for the histological analysis. The support of S. Svanberg and K. Svanberg is gratefully acknowledged. This work was financially supported by the Swedish Research Council for Engineering Sciences.

References

1. A. J. Welch, "The thermal response of laser irradiated tissue," IEEE J. Quantum Electron. **QE-20,** 1471–1481 (1984).
2. S. L. Jacques and S. A. Prahl, "Modeling optical and thermal distribution in tissue during laser irradiation," Lasers Surg. Med. **6,** 494–503 (1987).
3. M. Motamedi, S. Rastegar, G. LeCarpentier, and A. J. Welch, "Light and temperature distribution in laser irradiated tissue: the influence of anisotropic scattering and refractive index," Appl. Opt. **28,** 2230–2237 (1989).
4. W. Verkruysse, J. W. Pickering, J. F. Beek, M. Keijzer, and M. J. C. van Gemert, "Modelling the effect of wavelength on the pulsed dye laser treatment of port wine stains," Appl. Opt. **32,** 393–398 (1993).
5. C. Sturesson and S. Andersson-Engels, "A mathematical model for predicting the temperature distribution in laser-induced hyperthermia. Experimental evaluation and applications," Phys. Med. Biol. **40,** 2037–2052 (1995).
6. S. Thomsen, "Pathologic analysis of photothermal and photomechanical effects of laser–tissue interactions," Photochem. Photobiol. **53,** 825–835 (1991).
7. S. Rastegar and M. Motamedi, "A theoretical analysis of dynamic variation of temperature dependent optical properties in the response of laser irradiated tissue," in *Laser–Tissue Interaction*, S. L. Jacques, ed., Proc. SPIE **1202,** 253–259 (1990).
8. S. Thomsen, S. L. Jacques, and S. T. Flock, "Microscopic correlates of macroscopic optical property changes during thermal coagulation of myocardium," in *Laser–Tissue Interaction*, S. L. Jacques, ed., Proc. SPIE **1202,** 2–11 (1990).
9. G. J. Derbyshire, D. K. Bogen, and M. Unger, "Thermally induced optical property changes in myocardium at 1.06 mm," Lasers Surg. Med. **10,** 28–34 (1990).
10. S. Jaywant, B. C. Wilson, L. Lilge, T. Flotte, J. Woolsey, and C. McCulloch, "Temperature dependent changes in the optical absorption and scattering spectra of tissues: correlation with ultrastructure," in *Laser–Tissue Interaction IV*, S. L. Jacques and A. Katzir, eds., Proc. SPIE **1882,** 218–229 (1993).
11. J. W. Pickering, S. Bosman, P. Posthumus, P. Blokland, J. F. Beek, and M. J. C. van Gemert, "Changes in the optical properties (at 632.8 nm) of slowly heated myocardium," Appl. Opt. **32,** 367–371 (1993).
12. I. F. Cilesiz and A. J. Welch, "Light dosimetry: effects of dehydration and thermal damage on the optical properties of human aorta," Appl. Opt. **32,** 477–487 (1993).
13. J. W. Pickering, P. Posthumus, and M. J. C. van Gemert, "Continuous measurement of the heat-induced changes in the optical properties (at 1,064 nm) of rat liver," Lasers Surg. Med. **15,** 200–205 (1994).
14. R. Agah, A. H. Gandjbakhche, M. Motamedi, R. Nossal, and R. F. Bonner, "Dynamics of temperature dependent optical

properties of tissue: dependence on thermally induced alteration," IEEE Trans. Biomed. Eng. **43,** 839–846 (1996).
15. A. M. K. Nilsson, G. W. Lucassen, W. Verkruysse, S. Andersson-Engels, and M. J. C. van Gemert, "Changes in optical properties of human whole blood *in vitro* due to slow heating," Photochem. Photobiol. **65,** 366–373 (1997).
16. L. Liu, S. Andersson-Engels, C. Sturesson, K. Svanberg, C. H. Håkansson, and S. Svanberg, "Tumour vessel damage resulting from laser-induced hyperthermia alone and in combination with photodynamic therapy," Cancer Lett. **111,** 1–9 (1996).
17. A. M. K. Nilsson, R. Berg, and S. Andersson-Engels, "Measurements of the optical properties of tissue in conjunction with photodynamic therapy," Appl. Opt. **34,** 4609–4619 (1995).
18. J. W. Pickering, C. J. M. Moes, H. J. C. M. Sterenborg, S. A. Prahl, and M. J. C. van Gemert, "Two integrating sphere with an intervening scattering sample," J. Opt. Soc. Am. **9,** 621–631 (1992).
19. J. W. Pickering, S. A. Prahl, N. van Wieringen, J. F. Beek, H. J. C. M. Sterenborg, and M. J. C. van Gemert, "Double-integrating-sphere system for measuring the optical properties of tissue," Appl. Opt. **32,** 399–410 (1993).
20. A. Roggan, H. Albrecht, K. Dörschel, O. Minet, and G. J. Müller, "Experimental setup and Monte-Carlo model for the determination of optical tissue properties in the wavelength range 330–1100 nm," in *Laser Interaction with Hard and Soft Tissue II*, H. J. Albrecht, G. P. Delacretaz, T. H. Meier, R. W. Steiner, L. O. Svaasand, and M. J. van Gemert, eds., Proc. SPIE **2323,** 21–36 (1995).
21. J. R. Mourant, T. Fuselier, J. Boyer, T. M. Johnson, and I. J. Bigio, "Predictions and measurements of scattering and absorption over broad wavelength ranges in tissue phantoms," Appl. Opt. **36,** 949–957 (1997).
22. L. Wang and S. L. Jacques, "Monte Carlo modeling of light transport in multi-layered tissues in standard C," Report (Laser Biology Research Laboratory, M. D. Anderson Cancer Center, University of Texas, 1515 Holcombe Boulevard, Houston, Tex., 1992).
23. P. Parsa, S. L. Jacques, and N. S. Nishioka, "Optical properties of rat liver between 350 and 2200 nm," Appl. Opt. **28,** 2325–2330 (1989).
24. J. R. Zijp and J. J. ten Bosch, "Pascal program to perform Mie calculations," Opt. Eng. **32,** 1691–1695 (1993).
25. R. Graaff, J. G. Aarnoudse, J. R. Zijp, P. M. A. Sloot, F. F. M. de Mul, J. Greve, and M. H. Koelink, "Reduced light-scattering properties for mixtures of spherical particles: a simple approximation derived from Mie calculations," Appl. Opt. **31,** 1370–1376 (1992).
26. H. C. van de Hulst, *Light Scattering by Small Particles* (Wiley, New York, 1957).
27. W.-C. Lin, M. Motamedi, and A. J. Welch, "Dynamics of tissue optics during laser heating of turbid media," Appl. Opt. **35,** 3413–3420 (1996).
28. B. Beauvoit, T. Kitai, and B. Chance, "Contribution of the mitochondrial compartment to the optical properties of the rat liver: a theoretical and practical approach," Biophys. J. **67,** 2501–2510 (1994).
29. S. Bosman, "Heat-induced structural alterations in myocardium in relation to changing optical properties," Appl. Opt. **32,** 461–463 (1993).